Pergamon

Int. J. Solids Structures Vol. 35, No. 12, pp. 1241–1260, 1998

0020-7683/98 $19.00 + .00

PII: S0020-7683(97)00101-7

PARAMETER UNCERTAINTY AND DESIGN OF OPTIMAL EXPERIMENTS FOR THE ESTIMATION OF ELASTIC CONSTANTS

PER S. FREDERIKSEN†
Department of Solid Mechanics, Technical University of Denmark, DK-2800 Lyngby, Denmark

(*Received* 16 *July* 1996; *in revised form* 24 *March* 1997)

Abstract—This paper investigates an inverse technique for the identification of orthotropic elastic constants from measured plate natural frequencies. In general, the accuracy of the identified parameters depends on the method of estimation, modelling errors and measurement errors. The paper addresses the parameter uncertainty due to errors in the measurements. Based on assumptions of the measurement errors, second-order statistics of parameters are approximated by linearization schemes. The main focus is on the possibility of designing the experiment to minimize the uncertainty of the estimated parameters. The uncertainty of each estimate as function of the experimental design variables is investigated. Also the overall optimality of the experimental design defined as the hypervolume of the confidence region is considered. The results show that not all parameters are estimated with a sufficient precision in the general case, but by carefully designing the experiment, the parameter uncertainties can be greatly reduced. Both thin and thick plates are considered with focus on single-layer plates, but the results for laminated plates are also discussed. © 1998 Elsevier Science Ltd.

1. INTRODUCTION

Several different methods for deducing elastic material parameters from plate vibration have been proposed. In most studies, measured natural frequencies are used as the experimental data (Deobald and Gibson, 1988; Ayorinde and Gibson, 1993; Lai and Lau, 1993; Moussu and Nivoit, 1993; Pedersen and Frederiksen, 1992; Frederiksen 1992a; Sol, 1986; McIntyre and Woodhouse, 1988; Larsson, 1994), but methods have also been proposed which take measured mode shapes into consideration (Fällström, 1991; Fällström and Jonsson, 1991). The papers cited above, all address thin plates by employing the classical plate theory. Recently, also more advanced theories have been employed in order to extent the applicability and to extract out-of-plane parameters (Ayorinde, 1995; Frederiksen, 1992b, 1997a, 1997b). To verify the proposed methods, results have been compared with those obtained by approved classical test methods or those found in the literature. Additionally, a convincing agreement between model predictions and experimental measurements [see e.g. Larsson (1994); Frederiksen (1997b)] improves the confidence in a particular method. However, such approaches give only rough, qualitative indication of the accuracy of the method. In general, both systematic and random errors are present in the identified parameters. The errors depend on the method of estimation, modelling errors and measurement errors. Sol (1986) gave upper bounds on the parameter error caused by measurement errors, but the derivation was not based on statistics and excluded the correlation among parameters. Otherwise, none of the references, including those by the author, have presented an evaluation of the precision of the estimated values. The present work addresses this very important question, in that it is concerned with the random variability of the estimates caused by the presence of measurement errors. The estimation problem studied here concerns the determination of orthotropic elastic constants of composite plates from measured values of the plate natural frequencies. Both thin and thick plates are considered. In the case of thin plates, only the four in-plane elastic constants can be estimated, whereas for thick plates the two transverse shear moduli are estimated in addition. The estimation

† Current address for correspondence: RAMBØLL, Teknikerbyen 31, DK-2830 Virum, Denmark. E-mail: psf@ramboll.dk.

approach is detailed in previous work, covering both the theoretical (Frederiksen, 1997a) and the experimental aspects (Frederiksen, 1997b).

The first part of the present paper states the parameter estimation problem and presents the analysis of the parameter uncertainty. By this analysis, confidence regions and intervals can be specified in addition to the parameter estimates. This information is of utmost importance, not only to state the uncertainty in a specific experiment, but also to assess the robustness of the method in general. From a theoretical point of view, the analysis provides the means of searching for the best design of the experiment. This is the purpose of the final and main part of the paper. The best experiment is that providing the greatest precision or conversely the smallest uncertainty of the required parameters. Hence, the objective in the optimal experiment problem is to design the experiment to minimize the effect of errors on the estimated parameter values. The uncertainty of each estimate as function of the experimental design variables is studied, but also a criterion to indicate the overall optimal design involving all parameters is considered. This criterion is that of minimum volume of the confidence region for the parameters. The variables characterizing the experimental design are the plate aspect ratio, the length-to-thickness ratio, the direction of orthotropy for single-layer plates and the number of natural frequencies. Optimizing the experiment by taking all design variables simultaneously is not an amenable task. Furthermore, constraints on the variables often exist in practice. Therefore, this work is a parametric study of the individual parameter uncertainty as well as the overall optimality of the experimental design. Emphasis is placed on single-layer plates, but also results for laminated plates are discussed.

The results show that not all parameters are estimated with a sufficient precision in the general case, but by carefully designing the experiment, the parameter uncertainties can be greatly reduced. All results are obtained for a specific set of orthotropic elastic constants typical for composite materials. Even though the results are material dependent, the experimental design strategies obtained here are typical in a qualitative sense for orthotropic materials in general.

2. PLATE MODEL

The basis of the mathematical model for predicting the natural frequencies of the composite plate is briefly outlined. A rectangular plate of total thickness h, length a and width b is considered. A global reference co-ordinate system x-y-z is located at the middle plane, with the z-axis normal to this plane (see Fig. 1). The plate is composed of n layers of the same orthotropic material, each being oriented arbitrarily in the x–y plane. For each layer, a local co-ordinate system 1-2-3 is defined which coincides with the material symmetry axes. The primary direction of orthotropy 1 is chosen as the one of the two in-plane orthogonal directions with the larger modulus of elasticity. The angle between the x-axis and the 1-axis of layer i is the lamination angle or the direction of orthotropy and is denoted γ_i.

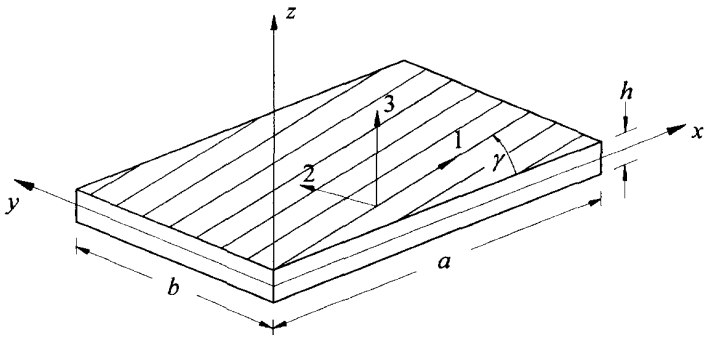

Fig. 1. Definition of structural and material co-ordinate systems.

The plate theory employed here is the higher-order shear deformation theory (HSDT) of Reddy (1984). It is based on the displacement field

$$u(x,y,z) = z\psi_x(x,y) - z^3\frac{4}{3h^2}\left(\frac{\partial w_0(x,y)}{\partial x} + \psi_x(x,y)\right)$$

$$v(x,y,z) = z\psi_y(x,y) - z^3\frac{4}{3h^2}\left(\frac{\partial w_0(x,y)}{\partial y} + \psi_y(x,y)\right)$$

$$w(x,y,z) = w_0(x,y) \tag{1}$$

where the two in-plane displacements of the midplane, u_0 and v_0, have been omitted, since the analysis is linear, limited to symmetric laminates and considers only the flexural modes of vibration. The displacement field (1) satisfies the condition of zero transverse shear strains on the top and bottom surfaces of the plate, but neglects the transverse normal strain.

Plane-stress reduced constitutive equations are employed. For an orthotropic material, these take the following form in the material co-ordinate system 1-2-3 (Whitney, 1987).

$$\begin{Bmatrix}\sigma_{11}\\ \sigma_{22}\\ \sigma_{12}\end{Bmatrix} = \begin{bmatrix} \dfrac{E_1}{1-\nu_{12}^2E_2/E_1} & \dfrac{\nu_{12}E_2}{1-\nu_{12}^2E_2/E_1} & 0 \\ \dfrac{\nu_{12}E_2}{1-\nu_{12}^2E_2/E_1} & \dfrac{E_2}{1-\nu_{12}^2E_2/E_1} & 0 \\ 0 & 0 & G_{12} \end{bmatrix} \begin{Bmatrix}\varepsilon_{11}\\ \varepsilon_{22}\\ \varepsilon_{12}\end{Bmatrix}, \quad \begin{Bmatrix}\sigma_{13}\\ \sigma_{23}\end{Bmatrix} = \begin{bmatrix} G_{13} & 0 \\ 0 & G_{23}\end{bmatrix}\begin{Bmatrix}2\varepsilon_{13}\\ 2\varepsilon_{23}\end{Bmatrix}. \tag{2}$$

Here, E_1 and E_2 are the two in-plane Young's moduli in the primary and secondary direction of orthotropy, respectively, G_{12} is the in-plane shear modulus, ν_{12} is the in-plane major Poisson's ratio and G_{13} and G_{23} are the transverse shear moduli. Note that the theory involves only six of the nine independent engineering constants which characterize an orthotropic material in three-dimensional configurations. The parameters which do not enter the theory are E_3, ν_{13} and ν_{23}. For layers with material directions that are not aligned with the plate co-ordinate system, rotational transformations (Whitney, 1987) are employed to obtain constitutive relations relative to the reference co-ordinate system x-y-z.

Plates with all edges free are considered in the present vibration problem. Closed form solutions of the employed higher-order theory cannot be obtained in this case. Instead, approximate solution are obtained using the Ritz method. Details and performance of the numerical model are described in Frederiksen (1995, 1997a). The present work also considers thin plates. For this purpose a similar Ritz model based on the classical plate theory (CPT) is used.

3. NONLINEAR ESTIMATION PROBLEM

The input quantities of the vibration model are classified into variables which are known or measurable quantities and parameters which are unknown constants. In the estimation problem, estimates of the parameters are obtained by using measured values of the input and output variables of the model. The independent (input) variables are the planform dimensions a and b, the thickness h, and the stacking sequence which for single-layer plates reduces to the single angle γ. The variables are contained in the vector $\mathbf{x}$, in the single-layer case defined by

$$\mathbf{x} = \{a, b, h, \gamma\}^{\mathrm{T}}. \tag{3}$$

Note that the material density ρ is not considered as a variable, but merely a numerical constant. The parameters, which are the unknown elastic constants, are contained in the vector $\boldsymbol{\theta}$ defined by

$$\boldsymbol{\theta} = \{E_1, E_2, G_{12}, \nu_{12}, G_{13}, G_{23}\}^{\mathrm{T}}. \tag{4}$$

In case where the model is based on the classical plate theory, the parameter vector is defined by the first four constants only. The dependent (output) variables are the I lowest plate natural frequencies f_i. The equations for prediction of the frequencies are formally written as

$$f_i = F_i(\mathbf{x}, \boldsymbol{\theta}), \quad i = 1, 2, \ldots I, \tag{5}$$

where i designates the frequency number. It is important to note that the functions F_i are nonlinear in the parameters $\boldsymbol{\theta}$.

In order to make statistical statements, several assumptions regarding the measurement errors are made. First, let there be additive, zero mean measurement errors in f_i. Secondly, it is assumed that the errors are uncorrelated, i.e. the covariance matrix of the errors is diagonal. Furthermore, the experience from the experimental work (Frederiksen, 1997b) suggests that the standard deviation of the measurement error is proportional to f_i, so that the variance is proportional to f_i^2. Therefore, it is assumed that the covariance matrix of the measurement errors is given by

$$\psi = \sigma^2 \operatorname{diag}[f_1^2 \quad f_2^2 \quad , \ldots, \quad f_I^2]. \tag{6}$$

where σ^2 is an unknown multiplicative constant. Additional assumptions are that there are no errors in the independent variables $\mathbf{x}$ and that $\boldsymbol{\theta}$ is a constant parameter vector with no prior information. Based on the theory of linear estimation, the weighted least-squares estimator should be applied under these assumptions (Beck, 1977), i.e. the estimates are obtained by minimizing the following objective function

$$\Phi(\boldsymbol{\theta}) = \sum_{i=1}^{I} \frac{(\hat{f}_i - f_i)^2}{\hat{f}_i^2} \tag{7}$$

where $\hat{f}_i$ is the measured value of f_i and the denominator f_i^2 has been replaced by $\hat{f}_i^2$ to avoid further nonlinearities in the minimization. It appears from eqn (7) that the approach is based on utilizing all the first I frequencies. However, there is no theoretical reason for this, it is purely to simplify the study. In practice one may wish to exclude certain frequencies in the range e.g. due to measurement difficulties.

Details of the minimization of Φ with respect to $\boldsymbol{\theta}$ are given in Frederiksen (1997a). It is important to note that optimal properties possessed by the estimator and the statistical quantities which can be derived based on the given assumptions in the linear case apply only approximately to the present non-linear model.

4. ANALYSIS OF PARAMETER UNCERTAINTY

At the optimal set of parameters $\boldsymbol{\theta}^*$, the objective function (7) attains its minimum $\Phi^* = \Phi(\boldsymbol{\theta}^*)$. For some small positive value ε, the ε-indifference region is defined by

$$\Phi(\boldsymbol{\theta}) - \Phi^* \leqslant \varepsilon. \tag{8}$$

Equation (8) defines a domain in the M-dimensional $\boldsymbol{\theta}$ space (M being the number of parameters) in which the rise in the objective function is considered insignificant compared

to Φ^*. The objective function Φ is approximated around its minimum using a second-order Taylor series expansion. It is assumed that $\boldsymbol{\theta}^*$ is an unconstrained minimum of Φ, therefore, the gradient vanishes and one obtains

$$\Phi(\boldsymbol{\theta}) \approx \Phi^* + \tfrac{1}{2}\delta\boldsymbol{\theta}^{\mathrm{T}}\mathbf{H}^*\delta\boldsymbol{\theta} \tag{9}$$

where $\delta\boldsymbol{\theta} = \boldsymbol{\theta} - \boldsymbol{\theta}^*$ and $\mathbf{H}^*$ is the Hessian of Φ at $\boldsymbol{\theta}^*$. At the minimum point, the Hessian is approximated by the Gauss method (Bard, 1974):

$$\mathbf{H}^* \approx \mathbf{N}, \quad N_{kl} = 2\sum_{i=1}^{I} \frac{1}{\hat{f}_i^2} \frac{\partial f_i}{\partial \theta_k}(\boldsymbol{\theta}^*) \frac{\partial f_i}{\partial \theta_l}(\boldsymbol{\theta}^*). \tag{10}$$

Analytical methods are used for the calculation of the first-order derivatives of the frequencies (Frederiksen, 1997a). Using eqns (8)–(10), the ε-indifference region is obtained as

$$\delta\boldsymbol{\theta}^{\mathrm{T}}\mathbf{N}\delta\boldsymbol{\theta} \leqslant 2\varepsilon \tag{11}$$

which is the equation of an M-dimensional ellipsoid.

To further assess the parameter interaction, the eigenvalue decomposition of $\mathbf{N}$ can be found

$$\mathbf{N} = \mathbf{Q}\boldsymbol{\Lambda}\mathbf{Q}^{\mathrm{T}} \tag{12}$$

where $\boldsymbol{\Lambda}$ is the diagonal matrix that contains the eigenvalues λ_i of $\mathbf{N}$, and $\mathbf{Q}$ is an orthogonal matrix whose columns are the normalised eigenvectors that form the M principal axes of the ellipsoid. The lengths of the principal axes are inversely proportional to the square roots of the eigenvalues. The longest axis defines the worst-determined direction in $\boldsymbol{\theta}$ space, and the shortest axis defines the best-determined direction (see Fig. 2). Observe that N_{kl}^{-1} denotes the k, l element of $\mathbf{N}^{-1}$ and not the reciprocal of N_{kl}.

With the covariance matrix of the measurement errors given by eqn (6), the covariance matrix of the estimates is approximated by (Bard, 1974)

$$\mathbf{V}_{\boldsymbol{\theta}} \approx 2\sigma^2\mathbf{N}^{-1} \tag{13}$$

where the unknown quantity σ^2 can be estimated using (Bard, 1974)

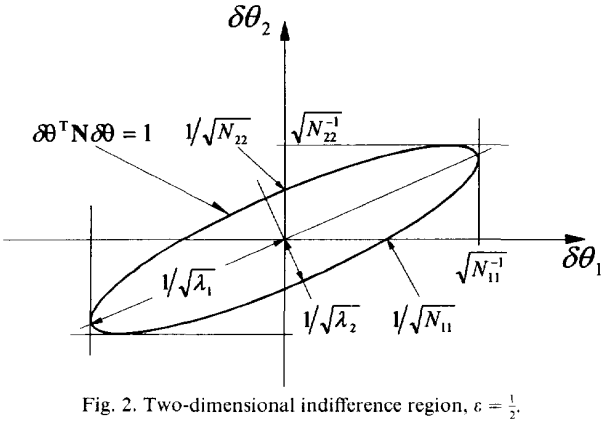

Fig. 2. Two-dimensional indifference region, $\varepsilon = \frac{1}{2}$.

$$\sigma^2 \approx \hat{\sigma}^2 = \frac{1}{I-M}\Phi^*. \tag{14}$$

A diagonal element V_{kk} of $\mathbf{V}_\theta$ is the variance of the estimated parameter θ_k, and an off diagonal element V_{kl} is the covariance between θ_k and θ_l that determines the correlation between parameters. The variance of a parameter estimate provides a measure of the precision of the estimated value. A large variance means that small variations in the data can affect the estimated value strongly and the precision of the estimate is poor. The square root of V_{kk} is the standard deviation of the kth parameter. The approximate correlation matrix can be obtained using the above equations. The k, l element of the correlation matrix is given by

$$\rho_{\theta_k,\theta_l} = \rho_{kl} = V_{kl}/\sqrt{V_{kk}V_{ll}}. \tag{15}$$

The reliability of the statistics obtained here is checked in Table 1 by a few comparisons with simulation results from Frederiksen (1997a). Zero mean, normally distributed measurement errors with three different levels, $\sigma = 0.5\%$, $\sigma = 1\%$ and $\sigma = 2\%$ are considered. The standard deviations obtained from the simulated results compare very well with the estimated values calculated from eqn (13), even for $\sigma = 2\%$. This indicates that the model is nearly linear in the parameters for variations in $\boldsymbol{\theta}$ affected by at least a few percent errors and thus, within this limit, the standard deviations are about proportional to the level of the experimental errors. The average bias obtained from the simulated results is, in all cases, small compared to the standard deviations of the estimates. Equation (14) provide on the average an excellent approximation of the experimental error since in the three cases, the average value of $\hat{\sigma}$ was found to be 0.497, 1.000 and 1.993%, respectively.

To obtain confidence regions and intervals, it is assumed that the errors in the measurements are normally distributed. Note that in this case, the maximum likelihood and the weighted least squares methods give the same estimator. Note also that the assumption that the error covariance matrix is known at least to within an arbitrary multiplicative constant is fundamental. Confidence regions which coincide with the indifference region of the objective function are chosen. With the model equations being nearly linear in the parameters around $\boldsymbol{\theta}^*$, the $100(1-p)\%$ joint confidence region is (Beck and Arnold, 1977)

$$\delta\boldsymbol{\theta}^{\mathrm{T}}\mathbf{N}\delta\boldsymbol{\theta} \leqslant 2M\hat{\sigma}^2 F_{1-p}(M, I-M) \tag{16}$$

where $F_{1-p}(M, I-M)$ is the $(1-p)$-fractile in the F-distribution with M and I–M degrees of freedom. For the sake of simplicity, one is frequently interested in the confidence interval for each parameter taken separately (Beck and Arnold, 1977)

Table 1. Monte-Carlo simulations for $I = 14$, $a/b = 2.64$, $a/h = 10$ and $\gamma = 0°$. Material properties: $E_2/E_1 = 0.1$, $G_{12}/E_1 = G_{13}/E_1 = 0.5$, $G_{23}/E_1 = 0.03$, $\nu_{12} = 0.3$. Normal distribution of errors

	E_1	E_2	G_{12}	ν_{12}	G_{13}	G_{23}
$\sigma = 0.5\%$						
Average bias (%)[a]	0.15	−0.09	0.03	0.98	−0.19	0.10
Std. dev. (%)[a]	1.31	1.50	1.07	20.0	1.39	3.37
Est. std. dev. (%)[b]	1.34	1.52	1.07	19.7	1.43	3.41
$\sigma = 1\%$						
Average bias (%)[a]	0.35	−0.20	0.06	−0.11	−0.35	0.50
Std. dev. (%)[a]	2.63	2.98	2.13	44.0	2.87	6.82
Est. std. dev. (%)[b]	2.67	3.04	2.13	39.5	2.87	6.83
$\sigma = 2\%$						
Average bias (%)[a]	0.64	−0.67	0.12	0.39	−0.55	3.08
Std. dev. (%)[a]	5.29	5.97	4.44	86.0	5.99	15.9
Est. std. dev. (%)[b]	5.34	6.08	4.26	79.0	5.74	13.7

[a] Simulation results from Frederiksen (1997a) based on 100 replications.
[b] $\sqrt{V_{kk}}$ from eqn (13).

$$|\delta\theta_k| \leqslant (V_{kk})^{1/2} t_{1-p/2}(I-M) \tag{17}$$

in which $t_{1-p/2}(I-M)$ is the $(1-p/2)$-fractile in the t-distribution with I–M degrees of freedom. Using eqns (13) and (14), eqn (17) can be expressed as

$$|\delta\theta_k| \leqslant (2\hat{\sigma}^2 N_{kk}^{-1})^{1/2} t_{1-p/2}(I-M). \tag{18}$$

5. EXPERIMENTAL DESIGN STRATEGIES

5.1. *Experimental design variables and constraints*

By designing the experiment is meant the choice of the values of $\mathbf{x}$ at which the I frequencies are to be observed. Note that the design does not include the shape and the boundary conditions of the plate since the rectangular shape is inherent in the model and the free boundaries are chosen to obtain accurate measurements (Frederiksen, 1997b). Since the problem is formulated in non-dimensional terms (Frederiksen, 1997a), the experimental design variables to be considered are the aspect ratio a/b and the length-to-thickness ratio a/h along with the material orientation γ for single-layer plates. Also, the number of frequencies I is considered as a design variable.

One should realise that in practice restrictions may be imposed on the variables. For example, the experimental equipment has limited frequency range which limits the number of frequencies to be measured. Also, a certain plate size is required to perform the measurement and since the thickness is fixed once the plate is fabricated, a restriction exist on the ratio a/h.

5.2. *Goodness of the experimental design*

The goal is to design the experiment in such a way that uncertainty is minimized. Therefore, the goodness of a particular experimental design is assessed by considering the confidence region as well as the uncertainty of each parameter. The quantity $\sqrt{N_{kk}^{-1}}$ is used to measure the uncertainty of the kth parameter. It relates to statistical quantities as it is proportional to both the standard deviation, the confidence interval (18) and the projections of the indifference or confidence region on to the θ_k axis, see Fig. 2 and eqns (11) and (16). For memo technical reasons, the notation $N_{kk}^{-1} = N_{\theta_k}^{-1}$ is used, which may be specified as for example $N_{\theta_4}^{-1} = N_{\nu_{12}}^{-1}$. Furthermore, normalized parameter values are used for the sake of parameter comparison. The indifference region for the relative parameters is defined by

$$\delta\bar{\boldsymbol{\theta}}^{\mathrm{T}} \bar{\mathbf{N}} \delta\bar{\boldsymbol{\theta}} \leqslant 2\varepsilon \tag{19}$$

where

$$\delta\bar{\theta}_k = \delta\theta_k/\theta_k^*, \quad \bar{N}_{kl} = N_{kl}\theta_k^*\theta_l^*. \tag{20}$$

Specifically, one obtains

$$\sqrt{\bar{N}_{\theta_k}^{-1}} = \sqrt{N_{\theta_k}^{-1}}/\theta_k \tag{21}$$

so the quantity $\sqrt{\bar{N}_{\theta_k}^{-1}}$ provides a measure of the relative uncertainty of the estimate, hence it is suitable for comparisons between parameters. The smaller the value of $\sqrt{\bar{N}_{\theta_k}^{-1}}$ the smaller the parameter uncertainty, however, the absolute value has no direct significance as long as σ^2 is unknown or an indifference size ε is not appointed. Note that the scaling in eqn (21) does not change the correlation coefficients (15).

As an overall criterion to assess the optimality of the experiment, it is chosen to consider the hypervolume of the confidence region in the normalized parameter space. Note that this implies that each parameter is equally important in a relative sense. The hypervolume is inversely proportional to the square root of the determinant of $\bar{\mathbf{N}}$ which equals the product of eigenvalues $\bar{\lambda}_i$ of $\bar{\mathbf{N}}$:

$$\text{Vol.} \propto \prod_{i=1}^{M} \sqrt{\bar{\lambda}_i^{-1}} = \sqrt{|\bar{\mathbf{N}}|^{-1}}. \tag{22}$$

Hence, the optimal experiment is the one which minimizes $\sqrt{|\bar{\mathbf{N}}|^{-1}}$ under given conditions. One should note that if the estimates are correlated, the confidence ellipsoid is rotated in space. A pure rotation does not affect the volume of the ellipsoid, but it does affect the individual $\bar{N}_{\theta_k}^{-1}$ as illustrated by Fig. 2.

For the theoretical study, the quantities $\sqrt{|\bar{\mathbf{N}}|^{-1}}$ and $\sqrt{\bar{N}_{\theta_k}^{-1}}$ can be determined from the model, taking $\hat{f}_i = f_i$ in eqn (10). Hence, no minimization of the objective function is performed. Instead, values of the material parameters, which defines the minimum point θ^*, are specified. The following set of non-dimensional orthotropic elastic constants is considered throughout this work

$$E_1 = 1, \quad E_2 = 0.1, \quad G_{12} = 0.05, \quad \nu_{12} = 0.3, \quad G_{13} = 0.05, \quad G_{23} = 0.03. \tag{23}$$

It is important to realise that the quantities (21) and (22) are material dependent due to the non-linearity of the problem. Therefore, the results presented here are not universal, but apply to this material only. However, in a qualitative sense the results are typical for orthotropic materials in general.

6. RESULTS

6.1. *Single-layer plates, classical plate theory*

Single-layer plates are treated in detail because they provide the most obvious test specimens and because they are comparatively simpler than general laminates in that they are characterized by a single angle γ. This section presents results for the four in-plane elastic constants based on the classical plate theory (CPT). Note that in this case, the uncertainty in terms of $\sqrt{\bar{N}_{\theta_k}^{-1}}$ is independent of h. This is because the estimation problem is non-dimensional in terms of the frequencies and non-dimensional frequencies are independent of h when obtained by the classical plate theory.

Figure 3 shows parameter uncertainties as functions of the aspect ratio for three different angles, $\gamma = 0$, 15 and 30°. The results are obtained for $I = 10$. Note that curves of this type are discontinuous because $\bar{\mathbf{N}}$ is a matrix derived from sensitivities. Discontinuity occurs when frequency number I and $I+1$ intersect and the corresponding modes switch place as a result of frequencies being ranged in a sequential order of magnitude. For $\gamma = 0°$ [Fig. 3(a)], the uncertainties of E_1, E_2 and G_{12} are about the same and varies little with the aspect ratio. The uncertainty in the estimation of Poisson's ratio differs radically. First, the curve is characterized by several pronounced local minima (the three most important are indicated by A, B, C). Second, the uncertainty is much larger (note the separate axis for ν_{12}). Curves similar to Fig. 3(a) are shown in Fig. 3(b, c) for $\gamma = 15$ and 30°, respectively. The off-axis angle has a beneficial effect on the estimation of ν_{12} in the sense that the precision is much less sensitive to the aspect ratio. Unfortunately, this is at the expense of the precision of the other parameters. For example, with $\gamma = 30°$, the uncertainty of G_{12} is about three times that for the plate with $\gamma = 0°$ for an aspect ratio between 1.2 and 2.2.

It is important to observe that the poor precision of ν_{12} that occurs between the minima in Fig. 3(a) does not significantly affect the precision of the other parameters. This is because the longest principal axis of the ellipsoid eqn (11) is nearly coincident with the ν_{12}-axis. Thus, there is little interaction between ν_{12} and the shear and Young's moduli. This has an important practical application, since E_1, E_2 and G_{12} can be estimated with high precision regardless of the precision of ν_{12}. Table 2 gives values of the uncertainties for two different values of the aspect ratio for a plate with $\gamma = 0°$. In addition, Table 2 considers the effect of taking ν_{12} as a fixed quantity (with the correct value) in the model. When the number of unknown parameters are reduced, the uncertainties of the remaining paramters decrease since correlation effects are reduced. For an aspect ratio where ν_{12} is ill-determined

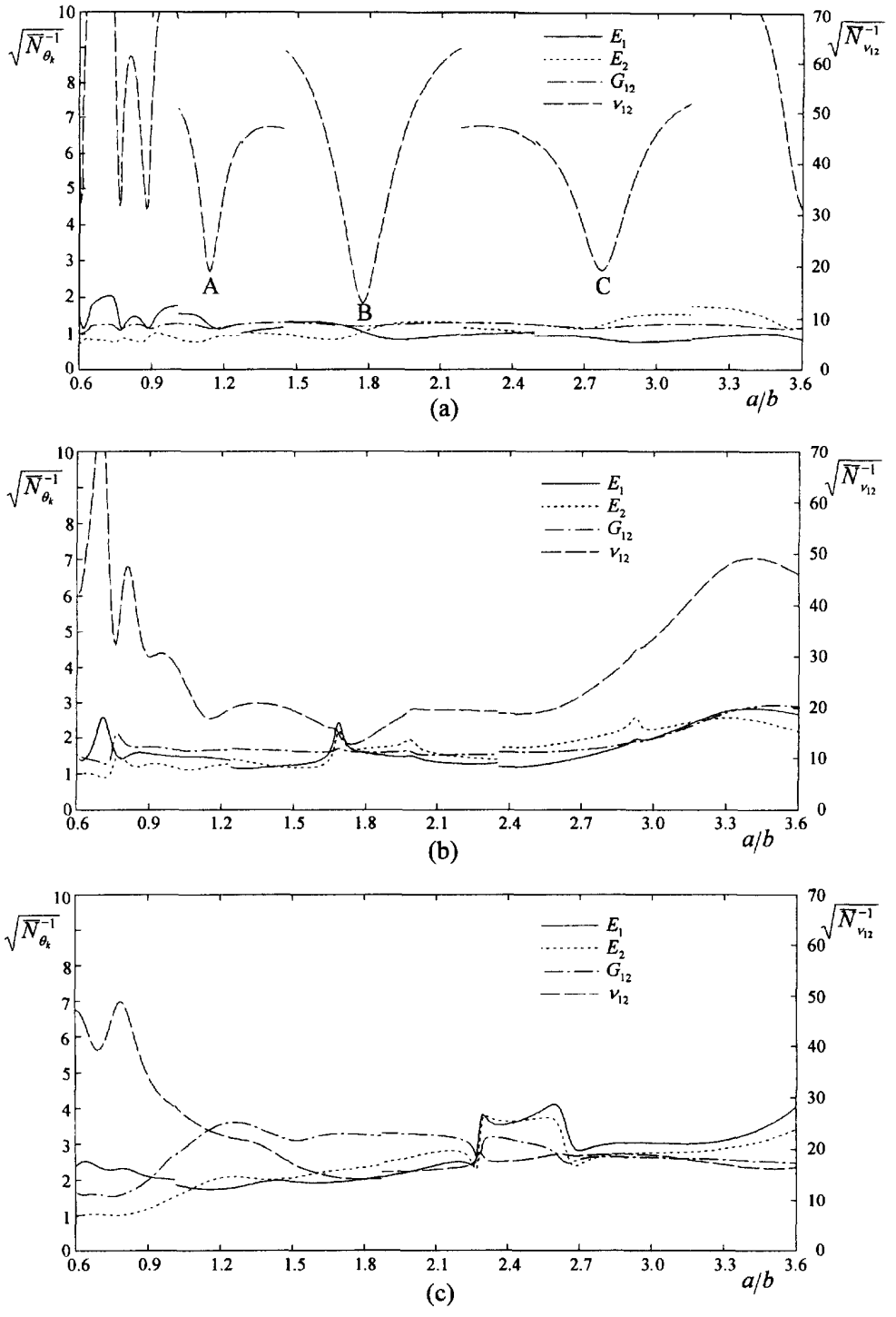

Fig. 3. Normalized parameter uncertainties vs aspect ratio for estimation of in-plane elastic constants of thin, single-layer plates, $I = 10$: (a) $\gamma = 0°$; (b) $\gamma = 15°$; (c) $\gamma = 30°$.

($a/b = 2.1$), especially the precision of E_2 can be improved by fixing ν_{12}, but for $a/b = 1.778$, which corresponds to point B in Fig. 3(a), the effect is negligible.

Figure 4 shows the overall optimality criterion as function of the aspect ratio for the three cases in Fig. 3. The optimal experimental design is confirmed to be a plate with $\gamma = 0°$ and an aspect ratio at point B. Minimum points A and C are nearly as good. A small angle

Table 2. Normalized parameter uncertainties at two different aspect ratios with and without estimation of ν_{12}, $I = 10$ and $\gamma = 0°$

Estimate ν_{12} ?	a/b	$\sqrt{\bar{N}^{-1}_{E_1}}$	$\sqrt{\bar{N}^{-1}_{E_2}}$	$\sqrt{\bar{N}^{-1}_{G_{12}}}$	$\sqrt{\bar{N}^{-1}_{\nu_{12}}}$
yes	1.778	1.06	1.06	1.21	13.0
no	1.778	1.06	1.04	1.21	—
yes	2.1	0.94	1.34	1.32	59.9
no	2.1	0.86	0.79	1.20	—

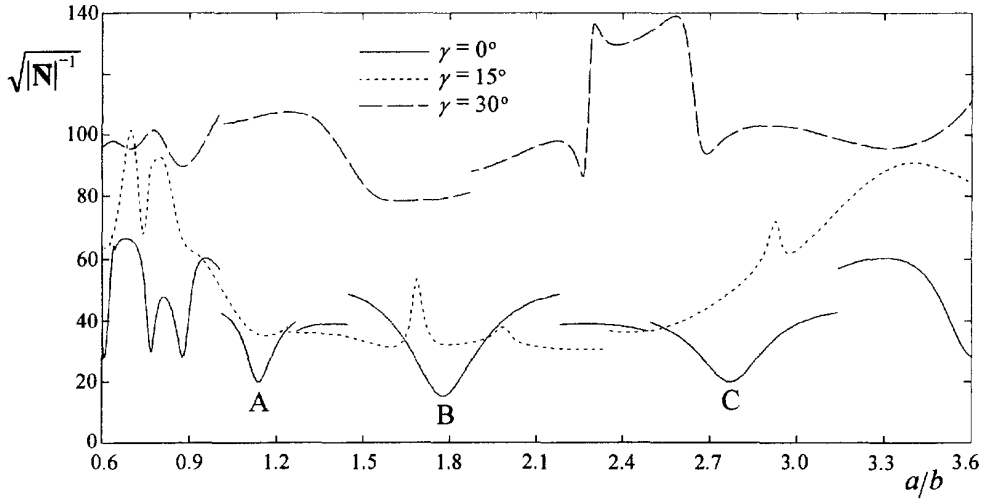

Fig. 4. Normalized volume of confidence region vs aspect ratio for estimation of in-plane elastic constants of thin, single-layer plates, $I = 10$.

($\gamma = 15°$) is advantageous only for aspect ratios between the minimum points of the plate having $\gamma = 0°$. Larger angles ($\gamma = 30°$) yield an overall significantly poorer experimental design.

The effect of the number of observations I on the uncertainties is studied in Fig. 5 for the plate with $\gamma = 0°$ and the aspect ratio of point B in Fig. 4. It is seen that including more frequencies in the estimation leads to smaller uncertainties. This is because each frequency adds new information not only in terms of a sensitivity coefficient for each parameter, but

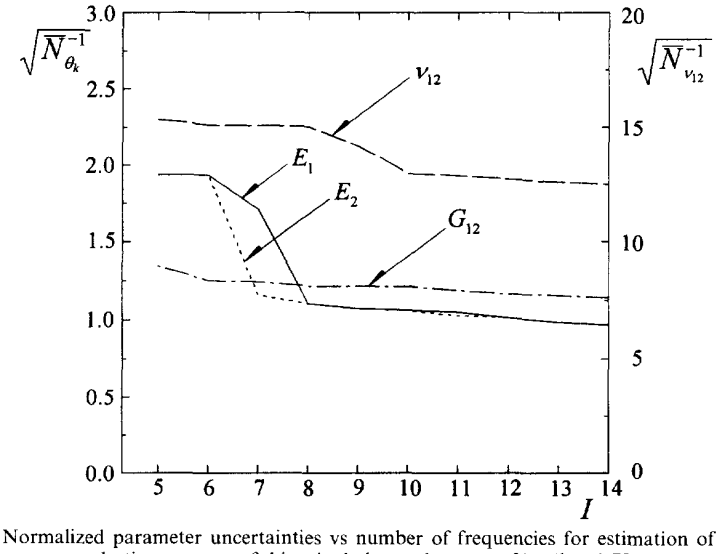

Fig. 5. Normalized parameter uncertainties vs number of frequencies for estimation of in-plane elastic constants of thin, single-layer plates, $\gamma = 0°$, $a/b = 1.78$.

also because correlation among the parameters is generally reduced. Since more frequencies improve the accuracy of the estimates, no value of I is optimal in terms of the overall design criterion (22), but the improvement is typically small beyond a certain value of I. In addition, since higher-order frequencies are generally predicted less accurately than lower ones, there is reason to include no more frequencies than actually necessary. Figure 5 shows that in the present case no significant reduction of $\sqrt{\bar{N}_{0_k}^{-1}}$ occurs for E_1, E_2 and G_{12} beyond the eighth frequency, whereas a slight improvement of the precision of ν_{12} is obtained for frequency number nine and 10. Thus, eight to 10 frequencies is appropriate when estimating the in-plane parameters of thin plates. It should be noted that according to eqns (16) and (18), the confidence region and intervals depend on I not only through $\mathbf{N}$, but also through the t and F statistics. The values of the t and F statistics decrease for increasing value of I, so for this reason more frequencies are desirable. Still, this effect alone is quite small, as one would observe from statistical tables.

Now, the minima A, B and C in Fig. 3(a) are examined in detail with respect to the estimation of ν_{12}. At each of these minima, the plate possesses a pair of mode shapes and associated frequencies that are particularly sensitive to Poisson's ratio. This is illustrated in Fig. 6 for point C where $a/b = 2.78$. Here, the fifth and sixth mode shapes have coincident frequencies for a zero value of ν_{12} [Fig. 6(a)]. (In the figure, the non-dimensional frequency is $\bar{f}_i = f_i a^2 \sqrt{\rho/E_1 h^2}$.) A positive value of ν_{12} has the effect of coupling the modes and separating the frequencies [Fig. 6(b)]. Therefore, the frequencies of these two modes are very sensitive to ν_{12}. Table 3 summarizes the characteristics of the three minimum points in Fig. 3(a). It is seen that with very close approximation, the aspect ratios creating the two-mode couplings are also those of the minima in Fig. 3(a) which are obtained for all 10

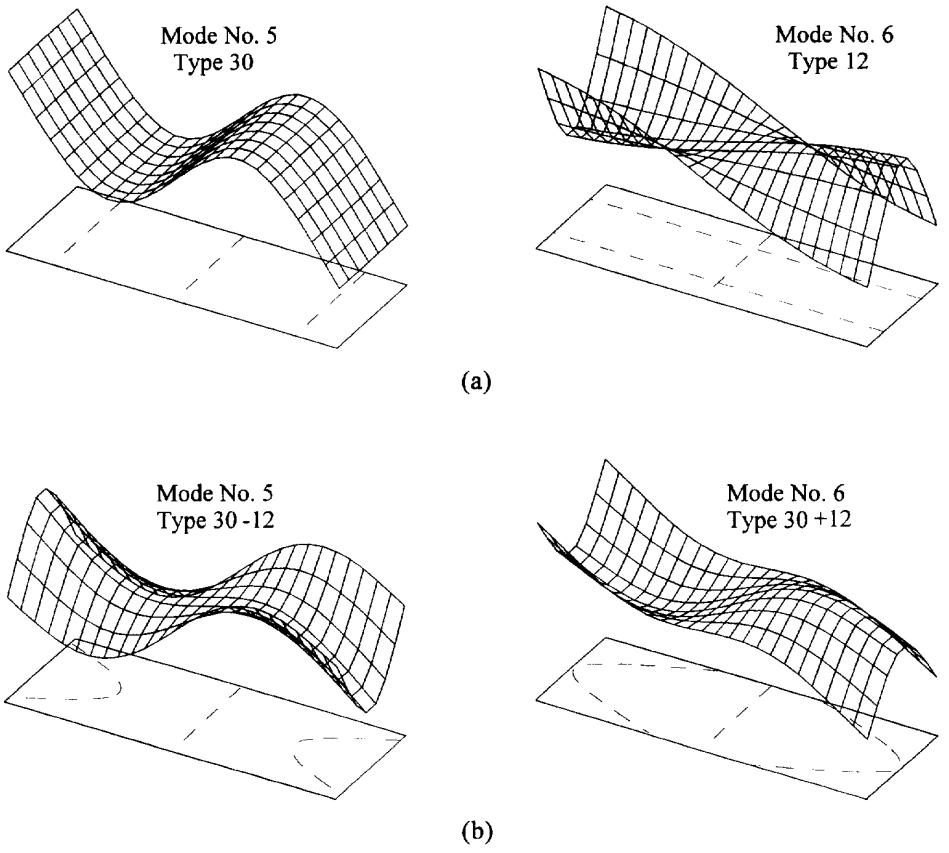

Fig. 6. Effect of Poisson's ratio on the fifth and sixth mode shape of a single-layer plate with $a/b = 2.78$, and $\gamma = 0°$. Dashed lines indicate nodal lines: (a) decoupled modes with coincident frequencies for $\nu_{12} = 0$, $\bar{f}_5 = \bar{f}_6 = 2.834$; (b) coupled modes with separated frequencies for $\nu_{12} = 0.3$, $\bar{f}_5 = 2.775$, $\bar{f}_6 = 2.915$.

Table 3. Important aspect ratios for the estimation of Poisson's ratio. Single-layer plate, $\gamma = 0°$

Optimal region [Fig. 3(a)]	a/b	$\sqrt{\bar{N}_{\nu_{12}}^{-1}}$	Most sensitive coupled modes mode numbers	mode types
A	1.139[a] 1.137[b]	18.9 19.0	5, 6	03−21, 03+21
B	1.776[a] 1.778[b]	13.0 13.0	2, 3	02−20, 02+20
C	2.773[a] 2.782[b]	19.1 19.2	5, 6	30−12, 30+12

[a] Minimum point in Fig. 3(a) based on 10 frequencies.
[b] Aspect ratio creating maximum coupling effect for the two modes in the last column.

frequencies. The coupling in point B is particularly simple because it involves the coupling of the first bending modes in the x- and y-directions. The maximum coupling in this case (equivalent to coincident frequencies for $\nu_{12} = 0$) is obtained for

$$a/b = (E_1/E_2)^{1/4}. \tag{24}$$

This is a well known relation that has been used for the determination of Poisson's ratio, [e.g. Sol (1986); McIntyre and Woodhouse (1988); Fällström (1991); Frederiksen (1992b)]. By contrast, the existence of the minima A and C is not well known. Unfortunately, a similar simple relation as eqn (24) for the coupling at point A and C in terms of the elastic constants cannot be given because the bending–twisting mode type depends on G_{12}. Also, the uncertainty of ν_{12} at these points are approximately 50% larger than that of the global minimum in point B. Failing to take an aspect ratio in the vicinity of one of the minima results in a very poor precision of Poisson's ratio, hence it is likely that the estimated value becomes completely erroneous (Deobald and Gibson, 1988). It should be noted that for an increasing degree of orthotropy, the shape of the minima becomes more narrow with increasing minimum values, leading in general to less reliable estimates of ν_{12}.

For the plate with $\gamma = 30°$, mode shapes that have high frequency sensitivities with respect to ν_{12} are not limited to specific aspect ratios. Therefore, ν_{12} can be estimated with reasonable precision over a wide range of a/b [Fig. 3(c)]. Figure 7 shows the two most important mode shapes for the estimation of ν_{12}, taking $a/b = 2$.

6.2. *Single-layer plates, higher-order plate theory*

This section presents results obtained with the HSDT-model. This model addresses thick plates and enables the estimation of the two transverse shear moduli in addition to the in-plane parameters. To assure a reasonable precision of the estimates of G_{13} and G_{23}, two more frequencies are included, i.e. the results are obtained for $I = 12$. Uncertainties of the in-plane and out-of-plane parameters versus aspect ratio for a plate with $a/h = 20$ and

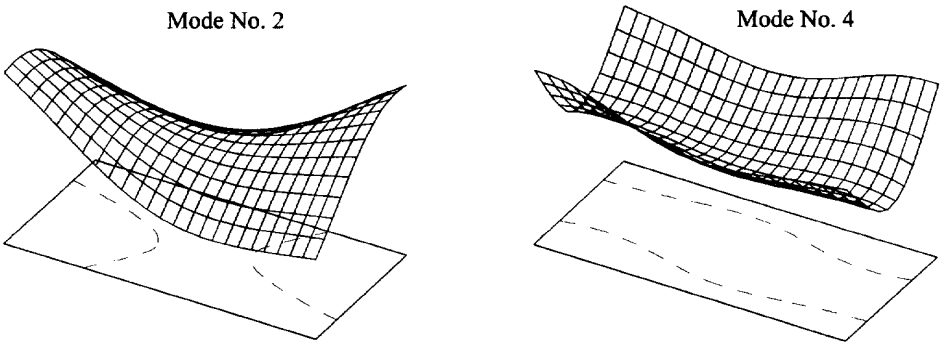

Fig. 7. Mode shapes possessing high frequency sensitivity with respect to Poisson's ratio. Single-layer plate, $\gamma = 30°$, $a/b = 2$ (dashed lines indicate nodal lines).

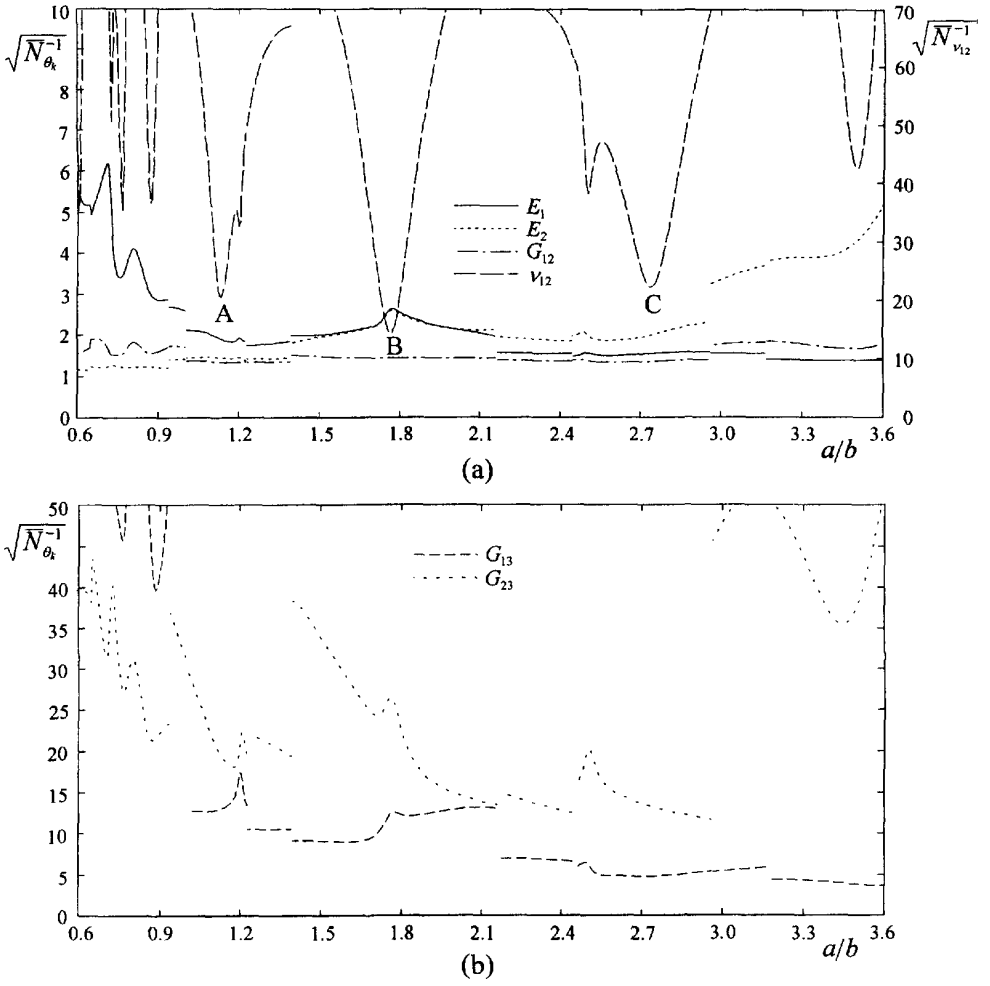

Fig. 8. Normalized parameter uncertainties vs aspect ratio for estimation of elastic constants of thick, single-layer plates, $\gamma = 0°$, $a/h = 20$ and $I = 12$: (a) in-plane elastic constants; (b) transverse shear moduli.

$\gamma = 0°$ are shown in Fig. 8(a, b). As regards the in-plane parameters, the observations drawn in the previous section hold qualitatively also for moderately thick plates. This is confirmed by the similarity between Figs 8(a) and 3(a). Particularly, the three characteristic minima A, B and C also exist in Fig. 8(a). It must be emphasized that due to the transverse shear effects, eqn (24) and the aspect ratios given in Table 3 apply only approximately to thick plates. Even though two more frequencies are included here, the uncertainties of the in-plane parameters are larger than those calculated with the CPT-model. This is not surprising since some correlation exist between the transverse shear moduli and the in-plane parameters. This is most pronounced for E_1 and E_2, whereas the uncertainties of G_{12} and ν_{12} are not significantly affected.

Next, the uncertainty of estimates of G_{13} and G_{23} is considered [Fig. 8(b)]. The precision of these estimates is closely related to the severity of the transverse shear effects on the plate vibration. Obviously, the particular mode associated with each frequency is of great importance. Bending-like modes in the x-direction have frequencies that are sensitive with respect to G_{13} and analogously in the y-direction. Because as many as 12 frequencies are considered, bending type modes in both directions occur. One should recall that transverse shear effects are more pronounced in materials that have a high ratio of in-plane Young's modulus to transverse shear modulus than those with a low ratio (e.g. isotropic materials). For the present material, which is typical for composites, this ratio is much higher in the 1-direction ($E_1/G_{13} = 20$) than in the 2-direction ($E_2/G_{23} = 3.33$). Because of this, the plate

possesses natural frequencies that are generally more sensitive with respect to G_{13} than to G_{23}. Therefore, as seen in Fig. 8(b), the estimate of G_{13} is generally more accurate than that of G_{23}.

When going further into details with Fig. 8(b) it is important to note that the curves are obtained for fixed values of a and h, i.e. a/b is varied by varying b only. The transverse shear effect of a particular mode is strongly dependent on the wavelength-to-thickness ratio. Since a/h is a fixed quantity whereas b/h decreases for increasing a/b, mainly modes dominated by bending in the y-direction are affected by varying a/b. This is the reason that the precision in the estimation of G_{23} improves whereas that of G_{13} is about constant for increasing a/b. This trend holds only locally, however. For increasing value of a/b (decreasing b), especially the frequencies of modes dominated by bending in the y-direction increases and this may cause these frequencies to gradually fall outside the fixed range of 12 frequencies. Such a situation occurs at $a/b = 1.39$. For an aspect ratio just below this value, the 12th mode is a pure bending mode in the y-direction. This mode is very sensitive to G_{23}, thus it contributes significantly to the estimation of G_{23}. When a/b is increased above this value, mode 12 and 13 switch place, the 12th mode now being dominated by bending in the x-direction. Consequently, a severe increase in the uncertainty of G_{23} is observed. The incident is repeated at larger aspect ratios, $a/b = 2.16$ and $a/b = 2.96$. Therefore, to obtain a high precision of both G_{13} and G_{23}, an aspect ratio about 2.9 is sensible. A larger value has an insignificant effect on the precision of G_{13}, but in return ruins the precision of G_{23}.

For comparison, Fig. 9 shows parameter uncertainties as functions of a/b for a plate with $\gamma = 30^\circ$. The parameters are estimated with less precision compared to the plate with $\gamma = 0^\circ$. The exception is the curve for ν_{12}, which resembles that of the CPT-model in Fig. 3(c). Note that the uncertainty of G_{13} is somewhat smaller than that of G_{23} which is due to the afore-mentioned higher ratio of in-plane Young's modulus to transverse shear modulus in the primary direction of orthotropy. Above $a/b = 1$, the correlation between G_{13} and G_{23} is high (≈ 0.9). This explains the parallel course of the two curves in Fig. 9(b). Generally, the correlation among parameters is much higher for plates with $\gamma \neq 0^\circ$ than for those with $\gamma = 0^\circ$. This is basically explained by the mode shapes. When material and plate axes do not coincide the mode shapes become more complicated as compared to the fairly simple bending and twisting like modes of orthotropic plates. Therefore, plates with $\gamma \neq 0^\circ$ as compared to those with $\gamma = 0^\circ$ have a smoother distribution of frequency sensitivities in the sense that each frequency is affected by all or nearly all parameters, but in return at less strength for each particular parameter. This situation causes high correlation among parameters. It is concluded that when using the HSDT-model, plates with off-axis material directions ($\gamma \neq 0^\circ$) provides a much poorer experimental design than does plates with $\gamma = 0^\circ$.

Now, returning to the case with $\gamma = 0^\circ$, Table 4 shows the correlations between the estimates for values of a/b representing point B and C in Fig. 8(a). Point B suffers from fairly high correlations between the estimates E_1, E_2, G_{13} and G_{23}. This interaction is responsible for the local rise in the uncertainty of all four parameters observed in Fig. 8(a, b). Other local peaks occurring at $a/b = 1.20$ and $a/b = 2.50$ are also due to a local rise in the correlation between the estimates. By contrast, with the aspect ratio of point C, the parameter correlation is much less. Only the correlations between E_1 and G_{13} and between E_2 and G_{23} have moderately high values. This seems inevitable because of the inherent coupling between the in-plane Young's modulus and the transverse shear modulus. Note also that ν_{12} correlates very little with any of the other parameters.

Figure 10 shows that overall, the optimal aspect ratio for the plate with $\gamma = 0^\circ$ is that corresponding to point C ($a/b = 2.74$). At this point the uncertainty of ν_{12} is at a local minimum [Fig. 8(a)] and the uncertainties of G_{13} and G_{23} are close to their global minimum values [Fig. 8(b)].

Curves similar to those in Figs 8 and 10 have also been calculated for $I = 13$ and $I = 14$. Apart from changing the points of discontinuity, changes occur mainly for G_{13} and G_{23}. For these estimates, the uncertainties are smaller and the curves flattens off somewhat rendering the uncertainties less affected by the aspect ratio as compared to the case with $I = 12$, but the general trend as seen in Fig. 8(b) does not change, i.e. an aspect ratio around

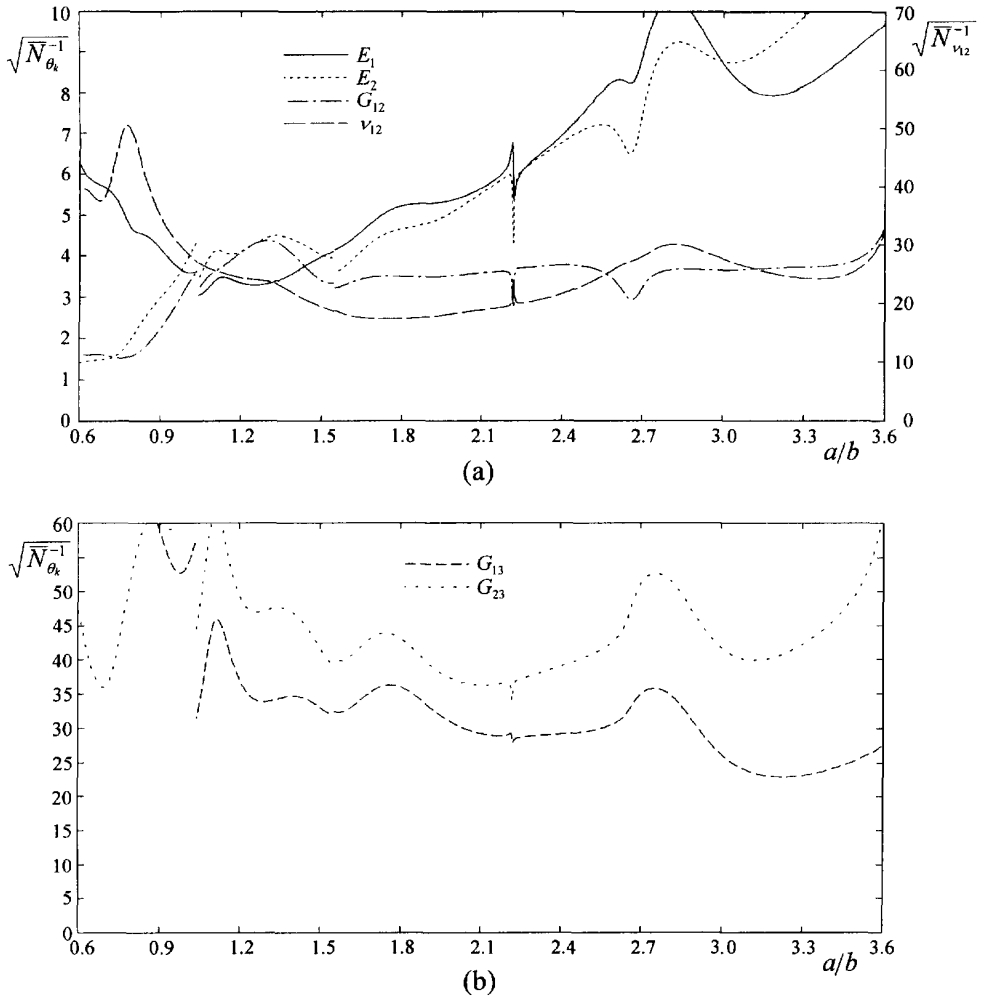

Fig. 9. Normalized parameter uncertainties vs aspect ratio for estimation of elastic constants of thick, single-layer plates, $\gamma = 30°$, $a/h = 20$ and $I = 12$: (a) in-plane elastic constants; (b) transverse shear moduli.

Table 4. Correlations $\rho_{\theta_k\theta_l}$ between estimates at two different aspect ratios, $\gamma = 0°$, $a/h = 20$ and $I = 12$

$\rho_{\theta_k\theta_l}$ θ_k / θ_l	E_2	G_{12}	ν_{12}	G_{13}	G_{23}
E_1	**−0.62**[a] −0.10[b]	**0.03** 0.05	**0.01** 0.01	**−0.90** −0.79	**0.61** 0.09
E_2	—	**0.17** 0.17	**0.02** −0.13	**0.60** 0.09	**−0.91** −0.85
G_{12}	—	—	**0.01** −0.05	**−0.15** −0.27	**−0.27** −0.25
ν_{12}	—	—	—	**−0.04** −0.11	**−0.12** 0.03
G_{13}	—	—	—	—	**−0.64** −0.11

[a] Values in bold obtained at $a/b = 1.769$ corresponding to minimum point B in Fig. 8(a).
[b] Values in normal obtained at $a/b = 2.740$ corresponding to minimum point C in Fig. 8(a).

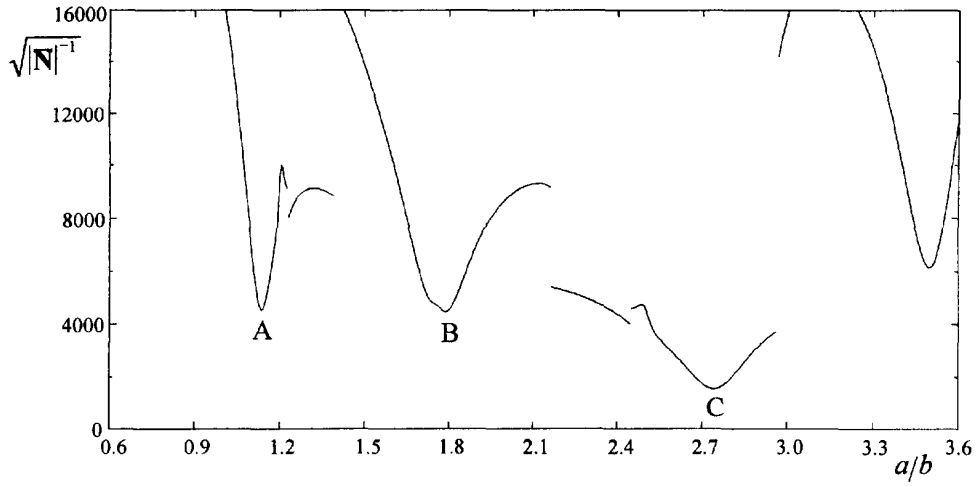

Fig. 10. Normalized volume of confidence region vs aspect ratio for estimation of elastic constants of thick, single-layer plates, $\gamma = 0°$, $a/h = 20$ and $I = 12$.

2.9 is still the best choice considering the precision of both G_{13} and G_{23}. Also the overall optimal aspect ratio is the same as that found for $I = 12$. It is interesting to note that the experimental results for two orthotropic plates presented in Frederiksen (1997b) were obtained with an aspect ratio in the vicinity of point B. Thus, the parameters G_{13} and G_{23}, which were of particular interest, were not estimated with optimal precision. The precision of these estimates could be greatly improved by taking a much larger aspect ratio. In the present case [Fig. 8(b)], the value of the normalized uncertainty for G_{23} decreases from 26.0 at point B to 13.2 at point C and that of G_{13} decreases from 12.6 to 4.8.

The effect of the length-to-thickness ratio on the parameter uncertainties is considered in Fig. 11 for a plate with $\gamma = 0°$. Aspect ratios are chosen corresponding to minima B and C in Fig. 8(a). Note that unlike the CPT-model, the corresponding values of a/b depend on a/h due to the transverse shear effect. In both figures, the uncertainties of the in-plane shear and Young's moduli are practically independent of a/h. In contrast, there is a strong improvement in the precision of G_{13} and G_{23} for decreasing a/h, which is due to the increased severity of the transverse shear effect. Still, the uncertainties are much larger than those of E_1, E_2 and G_{12} except for very thick plates. Comparing Fig. 11(a, b), it is seen that for a given value of a/h, all parameters except ν_{12} are estimated with greater precision for a/b chosen at point C than at point B. This is particularly the case for G_{13} and G_{23} which are

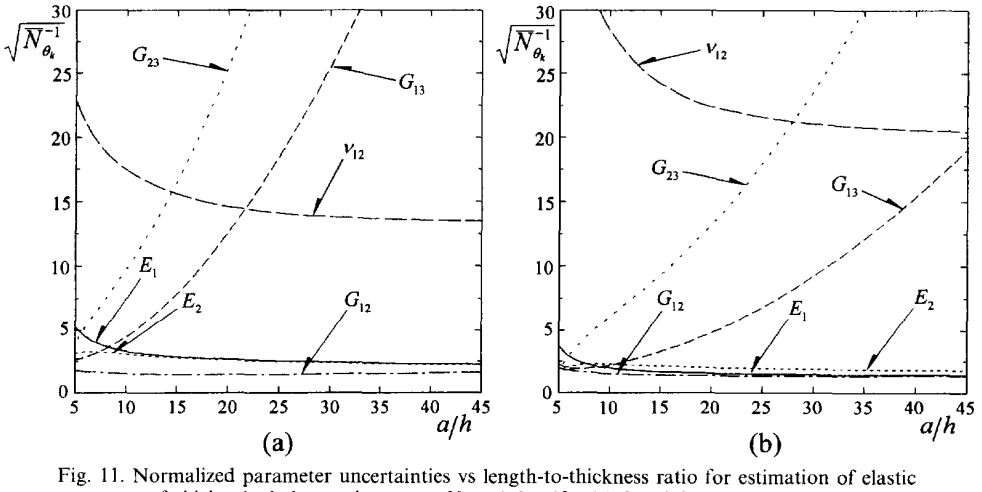

Fig. 11. Normalized parameter uncertainties vs length-to-thickness ratio for estimation of elastic constants of thick, single-layer plates, $\gamma = 0°$ and $I = 12$: (a) B minimum in Fig. 8(a); (b) C minimum in Fig. 8(a).

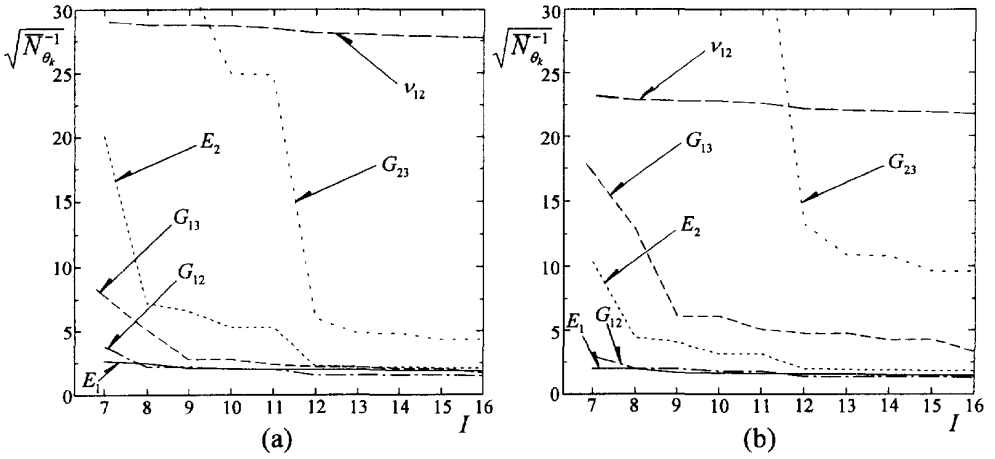

Fig. 12. Normalized parameter uncertainties vs number of frequencies for estimation of elastic constants of thick, single-layer plates, $\gamma = 0°$: (a) $a/h = 10$, $a/b = 2.64$; (b) $a/h = 20$, $a/b = 2.74$.

parameters of much interest. For a specified degree of precision of G_{13} and G_{23}, a much larger value of a/h can, therefore, be tolerated when a/b is taken corresponding to point C than to point B. This is an advantage not only from an experimental point of view but also because the error of the HSDT-model, which is neglected in this work, worsens for decreasing a/h.

The effect of the number of observations I on the uncertainties is studied in Fig. 12 for two different values of a/h. In each case, the value of a/b is taken as that which minimizes the quantity $\sqrt{|\tilde{\mathbf{N}}|^{-1}}$. As for the CPT-model (Fig. 5) more frequencies in the estimation leads to smaller uncertainties and beyond a certain value of I the improvement is small. The figure shows that higher-order frequencies are particularly important to obtain an acceptable precision of G_{23}. In order not to compromise the accuracy of the HSDT-model no more frequencies than are actually necessary should be included. Figure 12 shows that in the present case, 13 frequencies seems an appropriate choice for both values of a/h. Note that other materials and aspect ratios may lead to a different number.

6.3. *Laminated plates*

Since the model supports symmetric laminates composed of layers of the same orthotropic material, the estimation procedure and the calculations of the parameter uncertainties can be performed also for such plates. With respect to the length-to-thickness ratio and the number of frequencies the general results for single-layer plates also hold for laminates. Likewise, the experimental design can be optimized with respect to a/b. In general, however, laminates constitute a much poorer experimental design than single-layer plates. Nevertheless, it is relevant to investigate the parameter uncertainties of laminates since they are of interest in real tests. In this section some general aspects when considering laminated plates are discussed, supported by a few typical results.

The flexural vibration of plates is governed by the global plate bending stiffnesses. Because the different orientations of the layers in the laminate smoothens anisotropy in a global sense, certain changes in the elastic constants may have little effect on the bending stiffnesses as compared with single-layer plates. Therefore, compared with single-layer plates, the elastic constants of laminates are more difficult to identify from the frequencies, rendering less reliable estimates. As an example, consider a multi-layer cross-ply laminate. The effect of the parameter E_1 on the bending stiffnesses is about the same in the x- and y-directions because layers are oriented in both 0 and 90°. So is the case for E_2. Suppose E_1 and E_2 are increased and decreased, respectively, by the same magnitude, then the bending stiffnesses are very little affected and so are the frequencies. Similarly, the effect of decreasing G_{13} on the frequencies can, at least approximately, be eliminated by increasing G_{23} and vice versa. Because of this, estimation of the material parameters from natural frequencies of such plates is associated with very high correlation among these four parameters. It is

Table 5. Correlations ρ_{θ_k,θ_l} between estimates for eight-layer laminates, $a/h = 20$ and $I = 12$

ρ_{θ_k,θ_l} θ_k / θ_l	E_2	G_{12}	ν_{12}	G_{13}	G_{23}
E_1	−0.76[a] **−0.97**[b] *−0.39*[c]	−0.02 **0.12** *0.12*	−0.01 **0.66** *−0.10*	0.51 **0.81** *−0.66*	−0.70 **−0.84** *0.38*
E_2	—	0.06 **−0.12** *−0.75*	−0.42 **−0.70** *−0.09*	−0.84 **0.85** *0.49*	0.84 **0.85** *−0.67*
G_{12}	—	—	−0.09 **−0.03** *0.15*	−0.07 **−0.09** *−0.12*	−0.00 **−0.13** *0.28*
ν_{12}	—	—	—	0.31 **0.78** *0.39*	−0.32 **−0.77** *−0.34*
G_{13}	—	—	—	—	−0.93 **−0.99** *−0.87*

[a] Values in normal: cross-ply $[0°, 90°, 0°, 90°]_S$ laminate, $a/b = 1.84$.
[b] Values in bold: angle-ply $[45°, -45°, 45°, -45°]_S$ laminate, $a/b = 1.01$.
[c] Values in italic: angle-ply $[30°, -30°, 30°, -30°]_S$ laminate, $a/b = 1.23$.

Table 6. Normalized parameter uncertainties for eight-layer laminates, $a/h = 20$ and $I = 12$

Laminate	$\sqrt{\bar{N}^{-1}_{E_1}}$	$\sqrt{\bar{N}^{-1}_{E_2}}$	$\sqrt{\bar{N}^{-1}_{G_{12}}}$	$\sqrt{\bar{N}^{-1}_{\nu_{12}}}$	$\sqrt{\bar{N}^{-1}_{G_{13}}}$	$\sqrt{\bar{N}^{-1}_{G_{23}}}$
$[0°, 90°, 0°, 90°]_S$	2.07	17.0	1.37	39.7	21.6	27.4
$[45°, -45°, 45°, -45°]_S$	6.00	44.3	1.55	27.5	69.7	111.1
$[30°, -30°, 30°, -30°]_S$	1.76	7.61	3.81	18.8	21.9	37.8

readily seen that the more layers in the laminate and the closer the layers are oriented at 90° to each other, the more pronounced is this effect. Unbalanced laminates, i.e. laminates where coupling between bending and torsion exist, are particularly vulnerable, since as previously discussed for the single-layer case, this coupling further increases correlation among parameters. This renders the 45° angle-ply laminate particularly poor for the estimation of material parameters.

In Table 5 are shown the correlation coefficients obtained for eight-layer cross-ply and angle-ply laminates. As in the previous section, results are given for $a/h = 20$ and $I = 12$. The aspect ratio in each case is taken to be that which minimizes the quantity $\sqrt{|\bar{\mathbf{N}}|^{-1}}$. The cross-ply and the 45° angle-ply laminates have high interactions between the parameters, the latter being an exceptionally poor experimental design with values of ρ_{E_1,E_2} and $\rho_{G_{13},G_{23}}$ close to unity. As expected, the 30° angle-ply laminate has generally less correlation among parameters. In particular, this is the case for ρ_{E_1,E_2}. In return, an increased interaction between E_2 and G_{12} is observed. Corresponding normalized uncertainties for the three experimental designs are given in Table 6. A high correlation between E_1 and E_2 has a very severe effect on the relative precision of E_2 because E_1 is 10 times larger than E_2. This is particularly the case for the cross-ply and the 45° angle-ply laminates. For all three plates, estimates of E_1 and G_{12} are the most reliable. For the 45° angle-ply, uncertainties of the other four parameters are so large that the estimates will be useless.

As discussed in Section 6.2, the precision of the in-plane parameters is somewhat better when using the classical thin plate theory because fewer parameters are involved. Still, the trend observed with the advanced thick plate model also applies to the CPT-model, i.e. the results typically suffer from a very high correlation coefficient ρ_{E_1,E_2}.

7. DISCUSSION

In parameter estimation problems, calculating values of the estimates is only part of the solution. In order to assess the precision of the estimates, confidence regions should be

specified in addition. Here, an approximate analysis has been presented for the purpose of calculating confidence regions and intervals of material constants estimated from plate natural frequencies. The analysis relies on several statistical assumptions. Furthermore, the expressions are all approximate because the problem is nonlinear.

The method has been used to study theoretically the relative uncertainty of the estimates for different experimental designs using a fixed test material. The quantity used to measure the parameter uncertainty is the parameter standard deviation normalized by the measurement error. The investigation includes variations of aspect ratio, length-to-thickness ratio, direction of orthotropy and number of frequencies.

For single-layer plates, the in-plane Young's and shear moduli are very well-determined. The high reliability of G_{12} is of particular importance because G_{12} is difficult to measure by classical tests. Poisson's ratio is generally less well-determined. For the 0°-plate, a reliable estimate of ν_{12} is obtained only at specific aspect ratios where mode shapes are created that have high frequency sensitivities with respect to ν_{12}. Even in this case, the uncertainty of ν_{12} is about 10 times higher than those of E_1, E_2 and G_{12}. For plates with material axes different from the plate axes, the precision of ν_{12} is much less affected by the aspect ratio, but it is not better than the best obtained for the 0°-plate.

When estimating elastic constants of thick plates, particular attention must be paid to ensure a sufficient precision of the estimates of G_{13} and G_{23}. First, in order to improve the precision, it is very effective to reduce the length-to-thickness ratio. Second, a sufficient number of frequencies must be included, but taking frequencies beyond a certain number has limited effect. Finally, plates with material axes parallel to the plate axes are advantageous compared to plates having other material directions. For a 0°-plate with a/h less than about 15, the precision of G_{13} is comparable to that of the in-plane moduli, whereas the precision of G_{23} is slightly lower.

In the search for an optimal experimental design, the aspect ratio is a very important design variable because it has great impact on the vibration mode shapes which in turn are decisive for the frequency sensitivities. Overall, the best experimental design, i.e. that having the smallest hypervolume of the confidence region, is found for the single-layer 0°-plate. For thin plates, the optimal aspect ratio is that which yields equal bending stiffnesses in the directions of the plate axes, whereas for thick plates a significantly higher value is optimal. The optimal experimental designs are characterized by having little correlation among the parameters. The optimal design depends on the material parameters which are themselves the goal of the test. Thus, in practice the first experiment cannot be expected to provide estimates with minimum uncertainty, but the preliminary values may serve as a means of designing a better experiment where precision has been optimized either for individual parameters or taken as a whole. It is important to note that optimal values of the design variables (e.g. aspect ratio) generally varies for each parameter (see e.g. Fig. 8). Therefore, performing a single experiment which is optimal in an overall sense compromises the accuracy of individual parameters. To overcome this situation, different experiments which are optimized for individual elastic constants may be designed. It is stressed that even though the results given in this work are derived from a single test material, the qualitative results hold for a wide range of other orthotropic materials typical for composites.

The estimation of ply material constants of laminated plates is problematic. Typically, the parameters of such plates are highly correlated and tend to be inaccurate. The stacking sequence has great influence on the severity of this effect. In particular, the more layers in the laminate, the less reliable becomes the estimates. For certain lay-ups, it may well be found that some or most of the parameters are ill-determined. In this case the attention should be directed towards the global plate stiffnesses which may be deduced with a precision that is much better than that of the ply parameters. However, this is not further discussed in the present paper.

The type of inaccuracy studied here is that related to random errors in the frequency data. The present study has paid no considerations to model errors. An inexact model adds systematic errors to the estimates. One should bear in mind that in general, the smaller the value of a/h and the higher the frequency number the less accurate is both the CPT- and the HSDT-model. The effect of the CPT-model errors was already checked in Frederiksen

(1997a) for thin plates ($a/h \geqslant 50$) by using natural frequencies calculated with the more accurate HSDT-model. For thick plates, the inaccuracy of the HSDT-model itself may cause some systematic errors of the estimates, but to check the significance of these errors requires an even more accurate model.

REFERENCES

Ayorinde, E. O. (1995) Elastic constants of thick orthotropic composite plates. *Journal of Composite Materials* **29,** 1025–1039.

Ayorinde, E. O. and Gibson, R. F. (1993) Elastic constants of orthotropic composite materials using plate resonance frequencies, classical lamination theory and an optimized three-mode Rayleigh formulation. *Composite Engineering* **3,** 395–407.

Bard, Y. (1974) *Nonlinear Parameter Estimation.* Academic Press, New York.

Beck, J. V. and Arnold, K. J. (1977) *Parameter Estimation in Engineering and Science.* Wiley, New York.

Deobald, L. R. and Gibson, R. F. (1988) Determination of elastic constants of orthotropic plates by a modal analysis/Rayleigh–Ritz technique. *Journal of Sound and Vibration* **124,** 269–283.

Frederiksen, P. S. (1992a) Identification of temperature dependence for orthotropic material moduli. *Mechanics of Materials* **13,** 79–90.

Frederiksen, P. S. (1992b) Identification of material parameters in anisotropic plates—a combined numerical/experimental method. Ph.D. thesis, Department of Solid Mechanics, Technical University of Denmark, Denmark.

Frederiksen, P. S. (1995) Single-layer plate theories applied to the flexural vibration of completely free thick laminates. *Journal of Sound and Vibration* **186,** 743–759.

Frederiksen, P. S. (1997a) Numerical studies for the identification of orthotropic elastic constants of thick plates. *European Journal of Mechanics, A/Solids* **16,** 117–140.

Frederiksen, P. S. (1997b) Experimental procedure and results for the identification of elastic constants of thick orthotropic plates. *Journal of Composite Materials* **31,** 360–382.

Fällström, K.-E. (1991) Determining material properties in anisotropic plates using Rayleigh's method. *Polymer Composites* **12,** 306–314.

Fällström, K.-E. and Jonsson, M. (1991) A nondestructive method to determine material properties in anisotropic plates. *Polymer Composites* **12,** 293–305.

Lai, T. C. and Lau, T. C. (1993) Determination of elastic constants of a generally orthotropic plate by modal analysis. *International Journal of Analytical and Experimental Modal Analysis* **8,** 15–33.

Larsson, D. (1994) Dynamic evaluation of orthotropic material constants. Ph.D. thesis, Department of Structural Engineering, Chalmers University of Technology, Sweden.

McIntyre, M. E. and Woodhouse, J. (1988) On measuring the elastic and damping constants of orthotropic sheet materials. *Acta Metallurgica* **36,** 1397–1416.

Moussu, F. and Nivoit, M. (1993) Determination of elastic constants of orthotropic plates by a modal analysis/method of superposition. *Journal of Sound and Vibration* **165,** 149–163.

Pedersen, P. and Frederiksen, P. S. (1992) Identification of orthotropic material moduli by a combined experimental/numerical approach. *Measurement* **10,** 113–118.

Reddy, J. N. (1984) A simple higher-order theory for laminated composite plates. *Journal of Applied Mechanics* **51,** 745–752.

Sol, H. (1986) Identification of anisotropic plate rigidities using free vibration data. Ph.D. thesis, Free University of Brussels, Belgium.

Whitney, J. M. (1987) *Structural Analysis of Laminated Anisotropic Plates.* Technomic Publishing, Lancaster, PA.